

Optimization of laser printing of nanoparticle suspensions for microelectronic applications

Martí Duocastella · Heungsoo Kim · Pere Serra ·
Alberto Piqué

Received: 13 December 2011 / Accepted: 15 December 2011 / Published online: 7 January 2012
© Springer-Verlag (outside the USA) 2012

Abstract Digital printing of interconnects for electronic devices requires processes capable of delivering controlled amounts of conductive inks in a fast and accurate way. Laser-induced forward transfer (LIFT) is an emerging technology that enables controlled printing of voxels of a wide range of inks with micrometer resolution. Its use with high solids content nanoparticle suspensions results in the deposition of voxels shaped as the impinging laser beam. This allows higher processing speeds, increasing the throughput of the technique. However, the optimum conditions for printing spot-like voxels have not been determined, yet. In this work, we perform a systematic study of the main experimental parameters, including laser pulse energy, laser beam dimensions, and gap distance, in order to understand the role that these parameters play in laser printing. Based on these results, we find that there is a narrow fluence range at distances close to the receiving substrate where spot-like voxels are deposited. We also provide a detailed discussion of the possible mechanisms that may lead to the observed features.

1 Introduction

Non-lithographic processes have emerged as viable techniques for the digital printing of discrete patterns of diverse materials over different types of surfaces as required by most microelectronic devices. These low cost, relatively fast, and environmentally friendly alternatives to traditional photolithographic techniques have the potential of completely changing the way microelectronics are presently fabricated.

Examples of these digital printing techniques include inkjet [1] and laser-induced forward transfer (LIFT) [2]. Both of these techniques are capable of generating patterns comprising 3-dimensional pixels, or voxels, of precursor materials. These voxels usually contain suspensions of nanoparticles of the desired material that once printed must be processed via a low temperature (<250°C) curing step to evaporate the solvents, decompose any organic precursors that might remain in the dried voxel, and sinter the nanoparticles into larger grains to achieve the desired properties (electrical conductivity, optical transmission, etc.). Despite its broad appeal given its simplicity, inkjet is limited to the transfer of low viscosity, low solids loading nanoparticle suspensions in order to avoid clogging of the dispensing nozzles [1]. Because of this limitation, printing of precise patterns by inkjet is very difficult given the variable behavior of fluids on different types of surfaces and their resulting instability due to wetting effects [3]. Furthermore, the low concentration of solids in the inkjet-printed fluids results in concentration gradients during curing leading to significant variations in the thickness of the processed voxel.

Laser-induced forward transfer, also referred to as laser direct write (LDW), is another additive process in which controlled amounts of material are deposited from a donor film (or ribbon) to a receiving substrate by using laser

M. Duocastella · P. Serra
Departament de Física Aplicada i Òptica, Universitat de
Barcelona, Martí i Franquès 1, 08028 Barcelona, Spain

Present address:

M. Duocastella
Dept. of Mechanical and Aerospace Engineering, Princeton
University, Princeton, NJ 08544, USA
e-mail: mduocaste@princeton.edu

H. Kim · A. Piqué (✉)
Materials Science and Technology Division, Code 6364, Naval
Research Laboratory, Washington, DC 20375, USA
e-mail: pique@nrl.navy.mil

pulses [2]. Due to its nozzle-free nature, LIFT is capable of printing voxels with nanoinks of much higher viscosity than inkjet, thus significantly reducing variations between patterns due to wetting and drying effects [4]. LIFT of such nanoinks has been used recently to print voxels that reproduce the shape of the laser spot [5–9]. This process, referred to as laser-decal transfer, offers a revolutionizing approach to direct-writing techniques in which voxel shape and size become controllable parameters. The possibility to adapt the voxel shape according to the final pattern, such as using square voxels to obtain straight edges, allows an increase in the resolution and speed of the printing process. In addition, single voxels with the desired shape can be used to directly produce complex structures in one single printing step, reducing the processing time as well as avoiding problems related to the merging of multiple voxels as it occurs in most digital printing techniques [10]. Thus, printing spot-like voxels increases the capabilities of LIFT as well as its potential degree of parallelization [11].

Optimizing the printing of nanoinks by LIFT requires a better understanding of the behavior of the numerous parameters that affect this laser process. This work presents a study of the influence on the deposited voxels of some of these main parameters, including laser fluence, donor-receiving substrate separation, and laser beam spot size. For the purpose of this work, silver nanoparticle suspensions were used. These metallic nanoinks suspensions are well characterized and similar, but of higher viscosity than those typically used for inkjet. The morphology of the deposited voxels at the different conditions examined was evaluated using optical, confocal, and atomic force microscopy. This study has allowed determining the optimal conditions for the deposition of well-defined voxels that reproduce the shape of the irradiated area. Moreover, a discussion of the possible mechanisms involved in the laser forward transfer of nanoink suspensions under these conditions is also provided.

2 Experimental procedure

The laser forward transfer process used to print silver nanoinks (Cabot, CCI-300) in this work has been described elsewhere [4, 8]. Briefly, a small amount of silver nanoparticle ink (~ 14 cPs) was cast as a uniform layer (~ 1 μm thickness) using a wire coater (#2.5, Garner) onto a 7.5 cm diameter UV transparent quartz wafer and then dried in a vacuum oven at 50°C for 5 min to partially remove the volatile solvents, resulting in a nanoparticle ink with a viscosity of about 200 cPs. The ink coated side of the quartz wafer (referred to as donor film or ribbon) was placed above the receiving substrate (25 mm \times 25 mm \times 0.7 mm glass, Corning 1737) on the X–Y stage at a distance ranging from

~ 5 up to 125 μm . Both the donor film and the receiving substrate were translated by means of an X–Y motion control system (Aerotech, A3200).

A frequency-quadrupled Nd:YVO₄ (Coherent, AVIA) pulsed laser ($\lambda = 266$ nm and $\tau = 20$ ns FWHM) operating at 30 kHz was switched in amplitude and time by an acousto-optic modulator (AOM) to provide up to a few hundred μJ of pulse energy. The laser beam was then expanded to fill one of three different square apertures which were then imaged through a 10X objective to produce (as measured on polyimide) 12, 30, and 70 μm square spots, respectively. A CCD camera positioned to view along the same optical axis as the focusing objective provided a real-time plan view of the transfer process and sample. Using the CCD camera with the computer-driven X–Y stages (1 μm resolution) provided accurate visual placement and dimensioning of the fabricated structures. The laser fluence was varied from 20 to 80 mJ/cm^2 on the ribbon surface in order to study the mechanism of the laser forward transfer of silver nanoinks. The distance between the ribbon and the receiving substrate was also varied to study the transfer mechanism using polyimide spacers of three different thicknesses (13, 25, and 125 μm). After the structures had been transferred, both ribbon and substrate were cured on a hotplate at 150°C for 1 hour for further characterization.

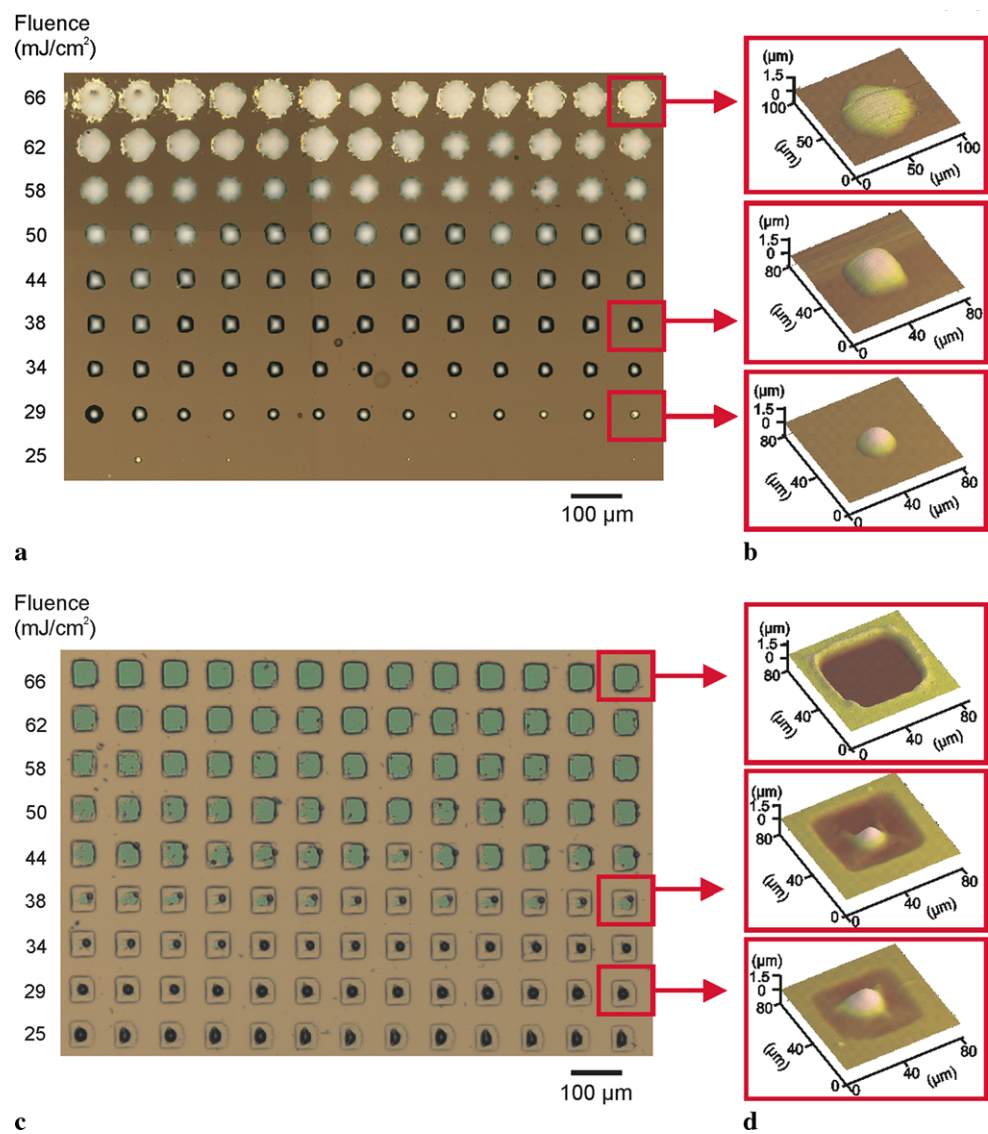
Optical microscopy (Olympus, BX51), confocal microscopy (Olympus, LEXT) and atomic force microscopy (AFM) (Digital Instruments, Dimension 3100) were used to characterize the surface morphology of both ribbons and transferred films.

3 Study of the influence of the main laser transfer process parameters

3.1 Laser fluence

In the first experiment, the influence of laser fluence on the morphology of the deposited material was analyzed through the preparation of an array with each feature printed with a single laser pulse, a ribbon to receiving substrate gap of ~ 5 μm , and each row obtained at a different fixed fluence (Fig. 1(a)). It can be observed that a minimum fluence of 29 mJ/cm^2 is required to deposit a feature, and the shape of the voxels changes with increasing fluence. First, at low fluences (29–34 mJ/cm^2) the features do not match the aperture but rather form a circular shape. Then at intermediate fluences (38–50 mJ/cm^2) they reproduce the square shape of the irradiated area. Finally, at high fluences (58–66 mJ/cm^2) the square shape is lost, the deposits become circular and debris surrounding the transfers appears. The laser fluence also affects the area covered by the deposits, with the largest features obtained at the highest fluences. As shown in Fig. 1(b),

Fig. 1 (a) Optical micrographs of the array prepared to study the influence of the laser fluence on the deposited features. (b) AFM images of representative features at each of the different fluence regimes. (c) Optical micrographs in transmission mode (using a green light source) of the donor film corresponding to the previous array. (d) AFM images of the spots on the donor film at each of the different fluence regimes. In all cases, the separation between the donor film and the receiving substrate was $5\ \mu\text{m}$



AFM images of laser-printed features from three different fluences (29, 38, and $66\ \text{mJ}/\text{cm}^2$) allow the above described morphological differences to be studied in more detail. The areas for each of the features generated from a laser-irradiated spot of $3000\ \mu\text{m}^2$ were calculated from these AFM images. The results indicated that the areas increased from about 350 to $1400\ \mu\text{m}^2$ and to $3000\ \mu\text{m}^2$ with increasing fluence. The AFM images also reveal the flattening of the deposits as the laser fluence increases. These results indicate that the optimum conditions for printing spot-like voxels are limited to the intermediate fluence region. It is interesting to notice though that at low fluences the reduction in area between deposited features and irradiated spots is almost an order of magnitude, suggesting the use of these conditions when higher resolutions are desired.

The corresponding donor film used for laser-printing the array in Fig. 1(a) was analyzed using optical microscopy in transmission mode (Fig. 1(c)). It can be observed that each

laser pulse generated a square spot of approximately the same size, indicating that the square aperture that shaped the top-hat laser beam was properly imaged on the donor film. Furthermore, three different regions can be distinguished, which can be directly correlated with those found in Fig. 1(a). More specifically, at low fluences ($<34\ \text{mJ}/\text{cm}^2$) remnants of nanoink forming a dark circular feature appear in the center of the spot, while at high fluences ($>50\ \text{mJ}/\text{cm}^2$) the material has been completely removed and thus only the green transmitted light is observed. Finally, at intermediate fluences material removal is only partial, and the central dark feature is still present, which in fact corresponds to a transition between the described behaviors. AFM images of three representative spots from each of the previous regions (Fig. 1(d)) reveal that the dark circular feature in the center of the spots obtained at low fluences is in fact a spike. The spike is surrounded by a depression of remaining material that extends until the limit of the irradi-

ated area. The outer border of such depression corresponds to the squared contour that appears in the spots of the lower rows of Fig. 1(c). As the fluence increases, the spike size diminishes and the depression becomes deeper, until at high fluences the whole irradiated area is completely removed with no material left.

The volume of the deposited material, as well as the volume removed from the ribbon, was quantified using confocal microscopy images of each feature and its corresponding spot. The average values for each fluence condition are plotted in Fig. 2. Up to 50 mJ/cm², the amount of deposited material increases with the laser fluence, as expected from the results of Fig. 1(a). The relationship between volume and fluence in this region seems quite linear, which is in good agreement with previous results of LIFT of low viscosity liquid solutions using Gaussian laser beams [12]. Above 50 mJ/cm², the amount of deposited material tends to be saturated. This corresponds to the situation of complete removal of the irradiated area: within this regime and for a top-hat beam, increasing the laser pulse fluence can only result in a higher kinetic energy of the transferred feature at the moment of impact, which increases the spreading and flattening of the feature but does not modify its volume. It is worth noting that for all the fluences analyzed the amount of removed material from the spots coincides quite well with the deposited volume within the margin of error, as it would be expected.

3.2 Gap separation

Three additional arrays were prepared in order to study the influence on the deposits of the gap between the donor film and the receiving substrate (Fig. 3). The arrays were obtained at the same fluence conditions as those of Fig. 1(a), but with three different gap separations (13, 25, 125 μm). The evolution of the morphology of the deposits with the laser fluence for 13 and 25 μm (Fig. 3(a) and 3(b)) is similar to that observed in Fig. 1(a), with the deposit of square-shaped features only at an intermediate fluence range. However, as the separation increases higher fluences are required to produce the same effects, as it can be clearly visualized with the shift towards upper fluences of the first deposited rows. The presence of debris also increases with the separation. Contrary to the previous cases (13 and 25 μm), at 125 μm (Fig. 3(c)) the deposited material does not reproduce the shape of the square-irradiated area at any of the fluence conditions. In fact, the deposits are elongated at low fluences and become circles with debris as the fluence is increased. These results demonstrate that, in contrast to the LIFT of aqueous solutions [13, 14], the current transfers are fairly sensitive to the separation between donor film and receiving substrate, and that the optimum printing conditions are achieved when the donor film is placed in very close proximity to the receiving substrate.

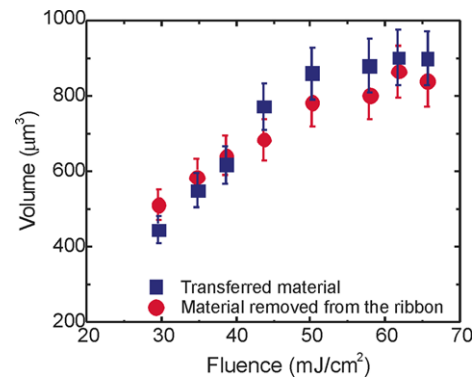


Fig. 2 Plot of the average volume in a row of both the deposited material and the material removed from the donor film versus the corresponding laser fluence

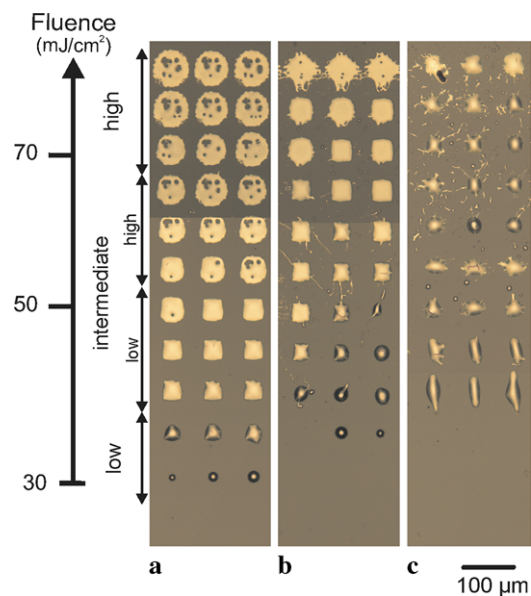


Fig. 3 Optical micrographs of three microarrays prepared varying the laser fluence from row to row, each one prepared at a different gap separation: (a) 13 μm, (b) 25 μm, (c) 125 μm

3.3 Aperture size

The micrographs from Fig. 4 show three arrays printed at a laser fluence of 50 mJ/cm², with a gap of 13 μm, each from a different size square-shaped aperture in order to analyze the effects of the aperture size on the deposits. The apertures used produced homogeneous square spots and the respective deposits were regular and well-defined squares with sizes of 12, 30, and 70 μm, respectively. From an application point of view, the greater than a factor of 5 scalability in voxel size that can be obtained with the laser transfer of nanoinks by simply adjusting the aperture size is remarkable and not achievable with other digital printing techniques.

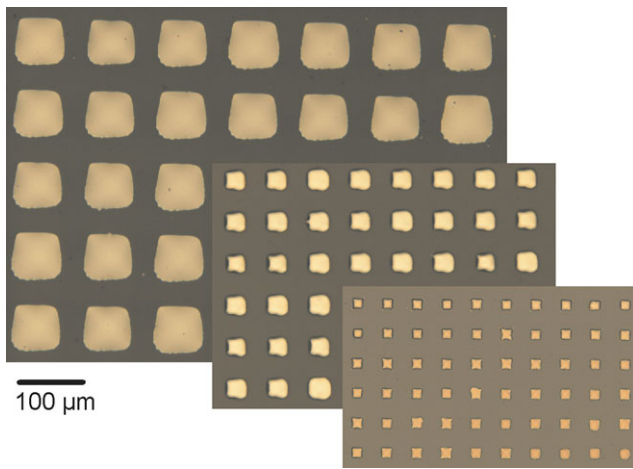


Fig. 4 Optical micrographs of three microarrays prepared at identical fluence conditions (50 mJ/cm^2) but using three different square-shaped aperture sizes imaged to produce 12, 30, and $70 \mu\text{m}$ square spots at the donor film. The separation between the donor film and the receiving substrate was $13 \mu\text{m}$

4 Discussion

The diversity of morphologies of the printed structures observed above can be interpreted recalling the time-resolved experiments of LIFT of aqueous solutions [13–17]. According to these works, the LIFT dynamics begin with the formation of a cavitation bubble that expands, and, depending on the experimental conditions, two main processes can occur: either the bubble while expanding makes contact with the receiving substrate [18], or if undisturbed, it further evolves into a jet, with the jet reaching the substrate [14]. It should be noted that there are significant differences between the present results and the previous LIFT experiments, such as the use of an ink with a different rheology, a smaller gap distance, and a different beam profile (top-hat versus Gaussian). Despite these differences, the fact that both techniques share the same configuration, together with some common trends in the evolution of the features morphology, seems to indicate that the deposition processes are similar. That being the case, all the multiple features obtained in the above experiments will be explained considering the bubble and jetting processes.

4.1 Bubble process

When a laser pulse reaches the donor film, the heating caused by its absorption induces the formation of a cavitation bubble. This bubble experiences initially a high internal pressure which favors its expansion. On the donor film surrounding the bubble though, there are forces that oppose this expansion, such as the surface tension and the atmospheric pressure. Initially, the bubble internal pressure is high enough to overcome these opposing forces and allow the bubble expansion. However, as the bubble expands,

the bubble internal pressure diminishes, which leads to its collapse [13]. If the receiving substrate is placed in close enough proximity to the donor film, it is possible for the expanding bubble to make contact with the substrate before it collapses completely. In this case, referred to as bubble process or BP, the donor film that surrounds the bubble is deposited on the substrate [18]. The cross-sectional area of the generated bubble will reproduce the shape of the irradiated area, which in this case corresponds to a square. Then, depending on the laser fluence, three conditions can be distinguished:

- Low-intermediate fluences or BP1 (Fig. 5(a)). Once the bubble contacts the receiving substrate, the bubble progressively cools down. This produces the collapse of the bubble from its sides, which are exposed to air, and turns the bubble into a filament. The filament is unstable due to surface tension, and finally breaks up. A fraction of this filament remains attached to the donor film, and recedes. For aqueous solutions, the remains of this filament disappear, being dragged by the surrounding liquid in the donor film, as it has been observed in time-resolved imaging experiments [13]. However, due to the higher viscosity of the nanoparticle ink used in this work, such a portion of the filament is not completely reabsorbed by the donor film, and appears as a spike in the AFM images (Fig. 1(d), 38 mJ/cm^2). Therefore, the observed spike can be considered as a snapshot of the final stage of the transfer process. In this regime, the deposited feature has a square shape. Since the bubble has a squared cross-sectional area, it produces a square deposit when it contacts the receiving substrate, while the contact area and shape of the bubble are preserved due to the high viscosity of the ink. This contrasts with the case of aqueous solutions, in which it is observed that the initial bubble contact area undergoes a shrinking process driven by its wettability with the receiving substrate [18]. This shrinking process is also accompanied by a rounding of the feature edges due to surface tension effects which cause the loss in shape of the initially irradiated spot. This comparison highlights the key role of rheology for the generation of features with different shapes in the laser printing of nanoinks.
- High-intermediate laser fluences or BP2 (Fig. 5(b)). This situation is similar to the previous one: the bubble contacts the receiving substrate and produces a square deposit. However, in this case the bubble completely detaches from the donor film due to its higher inertia. As a consequence, no material remains on the irradiated portion of the donor film and thus the filament observed in the previous case is not formed. This is consistent with the optical microscopy images at these conditions (Fig. 1(a) and 1(c), 50 mJ/cm^2).
- High laser fluences or BP3 (Fig. 5(c)). In this case, the generated bubble has a higher velocity than in BP1 or

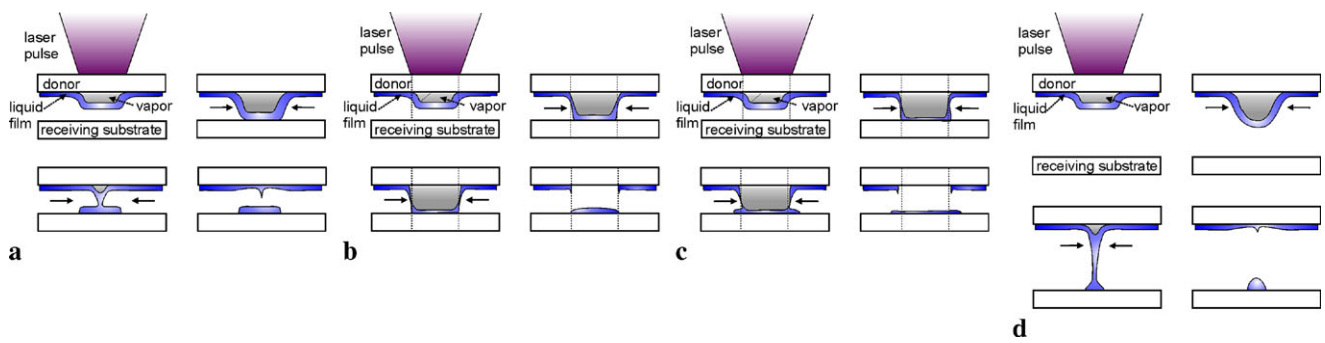


Fig. 5 Schematic representation of the different deposition processes that occur depending on the experimental conditions: bubble process at small gap separations and (a) low-intermediate fluences or BP1;

(b) high-intermediate fluences or BP2; (c) high fluences or BP3; (d) jet process at large gap separations and intermediate fluences or JP3

BP2. This produces a more violent impact of the bubble with the receiving substrate, which results in splashing. Consequently, the deposited ink does not maintain its original shape, but rather forms a circular spot with a size that surpasses the initially irradiated area. As a result of the violence of the process, debris can also be generated. The AFM images in Fig. 1(b) and 1(d), at a fluence of 66 mJ/cm^2 , correspond to this situation.

4.2 Jet process

As commented before, the generated cavitation bubble is not stable, but tends to collapse over time. Thus, if the receiving substrate is placed at a distance far enough to avoid the bubble contact, the bubble collapses completely. The collapse preferentially occurs along the bubble sides, whereas the central tip of the bubble maintains its progression due to its inertia. As a result of this asymmetric collapse, a thin jet is fully developed. This jet advances until finally reaching the receiving substrate, where it deposits its material. This case is referred to as jet process or JP. In spite of the initial squared shape of the bubble, the resulting jet acquires a circular cross-section due to the transversal component of the surface tension, which tends to favor such geometry in order to minimize the surface energy of the jet. The same would apply for any other shape: the bubble collapses at the expense of losing its initial shape. Depending on the laser fluence, four different situations can be distinguished:

- Very low laser fluences or JP1. Once the jet is formed, its inertia is not high enough to overcome the axial component of its surface tension, and thus the jet stops moving forward and recedes back to the ribbon substrate. If the gap separation is larger than the maximum jet length, no material is deposited on the receiving substrate, since the jet cannot reach it. Otherwise, a circular feature is deposited (Fig. 3(a), 29 mJ/cm^2). Since the maximum jet length increases with laser fluence, this explains the increment in the deposition threshold as the gap separation is increased (Fig. 3).

- Low laser fluences or JP2. In this situation, the jet inertia overcomes the surface tension forces and in the absence of a receiving substrate the jet continues advancing until breakup [13]. Two different situations should be distinguished. The first one corresponds to the case in which the jet is able to reach the receiving substrate before breakup. This occurs for relatively small gap separations, and results in the deposition of regular circular features, according to the aforementioned effect of the transversal component of surface tension. The first rows from the bottom in Fig. 3(b) correspond to this case. The second situation occurs when the jet breaks up before reaching the receiving substrate. This situation can lead to different shapes, from circular droplets to splashing. In fact, the elongated shapes obtained in the first rows of Fig. 3(c) could be attributed to one of these possibilities. In this case, the kinetic energy of the jet is low due to the low fluences employed. Thus, when the jet breaks up before contacting the receiver, parts of the jet can easily be deflected from the vertical direction, producing the observed elongated features.
- Intermediate laser fluences or JP3 (Fig. 5(d)). For this condition it is necessary to analyze the different configurations depending on the gap separation. At small gap separations, as already described, a square feature is deposited due to the bubble process. The bubble, though, tends to collapse over distance. Thus, as the gap separation is increased, the bubble reaches the receiving substrate while undergoing partial collapse. Such collapse may not be enough to completely erase the initial bubble shape, but accounts for its shrinkage. This explains the reduction in size of the features deposited in the third and fourth rows of Fig. 3(b), when compared to the square features deposited at the same fluence but at a gap distance of $13 \mu\text{m}$ (Fig. 3(a)). When the gap separation is further increased, the collapse of the bubble into a jet is complete, and thus the square shape is lost, as shown schematically in Fig. 5(d). Therefore, only circular features can

be deposited, as it is observed in the intermediate energy range at a separation of 125 μm (Fig. 3(c)). The presence of some debris can be attributed to the higher jet speed, which would produce some splashing when impinging on the receiving substrate surface.

- High laser fluences or JP4. Again, depending on the gap separation different configurations are expected. At small gap separations, the bubble process progresses as in BP3. However, as the gap separation increases, the ink spreads over a smaller area, due to the collapse of the bubble into a jet (top rows of Fig. 3(b)). Finally, at very large separations, the bubble has fully collapsed into a high-speed jet which upon impact on the receiving substrate generates a circular feature with debris. This corresponds to the top rows of Fig. 3(c).

A schematic summary of the conditions that lead to the different printing mechanisms and voxel morphologies is presented in Fig. 6. Printing well-defined and controllable voxels requires small gap separations between the donor and the receiving substrate. At these conditions, two compact and well-defined types of shapes can be obtained corresponding to low and intermediate fluences. At low fluences, circular voxels are printed with the jetting process (JP2), independent of the shape of the laser spot. This situation can be exploited for maximizing the resolution of LIFT, since the size of the printed voxel is smaller than the irradiated area. At intermediate fluences, spot-like voxels corresponding to the laser pulse shape are printed with the bubble process (BP1 or BP2). These are the optimum conditions for laser printing of nanoinks where voxel shape and size become controllable parameters. This capabilities make LIFT unique, since no other digital printing technique allows such degree of control on the material being deposited.

5 Conclusions

The morphological characterization of nanoparticle suspensions deposited by laser induced forward transfer under different conditions has allowed determining the optimum conditions for printing features with the same shape as the irradiated spot. It has been found that this technique is very sensitive to laser fluence and gap separation, achieving truly spot-like transfers within a narrow fluence range with the receiving substrate situated very close to the donor film. These constraints can be understood considering that the spot-like transfer process is achieved by the contact of a laser generated cavitation bubble with the receiving substrate with a minimum impact force. Due to the rheology of the ink, the initial bubble contact area is maintained in the overall process, which allows preserving the shape of the irradiated spot in the deposits. When these conditions are met, it is possible to obtain features with different shapes and sizes by

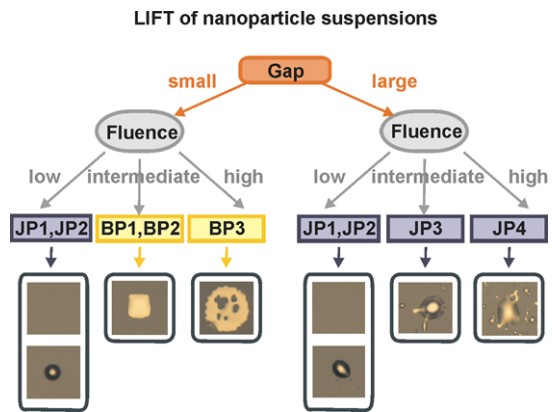


Fig. 6 Scheme of the deposition processes and voxel shapes corresponding to the various printing conditions described in the text

simply changing the laser irradiated spot. Thus, combining this technique with beam shaping methods offers a promising approach for the rapid prototyping of microelectronic devices.

Acknowledgements This work has benefitted from a research program funded by MCI of the Spanish Government (Projects MAT2010-15905 and CSD2008-00023), and Fondo Europeo de Desarrollo Regional (FEDER). The Office of Naval Research sponsored part of this work.

References

1. P. Calvert, Inkjet printing for materials and devices. *Chem. Mater.* **13**, 3299–3305 (2001)
2. C.B. Arnold, P. Serra, A. Piqué, Laser direct-write techniques for printing of complex materials. *Mater. Res. Soc. Bull.* **32**, 23–31 (2007)
3. H. Kang, D. Soltman, V. Subramanian, Hydrostatic optimization of inkjet-printed films. *Langmuir* **26**, 11568–11573 (2010)
4. R.C.Y. Auyeung, H. Kim, S.A. Mathews, A. Piqué, Laser direct-write of metallic nanoparticle inks. *J. Laser Micro Nanoeng.* **2**, 21–25 (2007)
5. J. Wang, R.C.Y. Auyeung, H. Kim, N.A. Charipar, A. Piqué, Three-dimensional printing of interconnects by laser direct-write of silver nanopastes. *Adv. Mater.* **22**, 4462–4466 (2010)
6. H. Kim, R.C. Auyeung, S.H. Lee, A.L. Huston, A. Piqué, Laser-printed interdigitated Ag electrodes for organic thin film transistors. *J. Phys. D, Appl. Phys.* **43**, 085101 (2010)
7. A. Piqué, R.C.Y. Auyeung, H. Kim, K.M. Metkus, S.A. Mathews, Digital microfabrication by laser decal transfer. *J. Laser Micro Nanoeng.* **3**, 163–169 (2008)
8. H. Kim, R. Auyeung, S. Lee, A. Huston, A. Piqué, Laser forward transfer of silver electrodes for organic thin-film transistors. *Appl. Phys. A, Mater. Sci. Process.* **96**, 441–445 (2009)
9. H. Kim, J.S. Melinger, A. Khachatryan, N.A. Charipar, R.C.Y. Auyeung, A. Piqué, Fabrication of terahertz metamaterials by laser printing. *Opt. Lett.* **35**, 4039–4041 (2010)
10. D. Soltman, B. Smith, H. Kang, S.J.S. Morris, V. Subramanian, Methodology for inkjet printing of partially wetting films. *Langmuir* **26**, 15686–15693 (2010)
11. R. Auyeung, H. Kim, N. Charipar, A. Birnbaum, S. Mathews, A. Piqué, Laser forward transfer based on a spatial light modulator. *Appl. Phys. A, Mater. Sci. Process.* **102**, 21–26 (2011)

12. M. Colina, M. Duocastella, J.M. Fernandez-Pradas, P. Serra, J.L. Morenza, Laser-induced forward transfer of liquids: Study of the droplet ejection process. *J. Appl. Phys.* **99**, 084909 (2006)
13. M. Duocastella, J.M. Fernandez-Pradas, J.L. Morenza, P. Serra, Time-resolved imaging of the laser forward transfer of liquids. *J. Appl. Phys.* **106**, 084907 (2009)
14. M. Duocastella, J.M. Fernandez-Pradas, J.L. Morenza, P. Serra, Sessile droplet formation in the laser-induced forward transfer of liquids: A time-resolved imaging study. *Thin Solid Films* **518**, 5321–5325 (2010)
15. M. Duocastella, J.M. Fernandez-Pradas, P. Serra, J.L. Morenza, Jet formation in the laser forward transfer of liquids. *Appl. Phys. A, Mater. Sci. Process.* **93**, 453–456 (2008)
16. C. Unger, M. Gruene, L. Koch, J. Koch, B. Chichkov, Time-resolved imaging of hydrogel printing via laser-induced forward transfer. *Appl. Phys. A, Mater. Sci. Process.* **103**, 271–277 (2010)
17. M. Brown, N. Kattamis, C. Arnold, Time-resolved dynamics of laser-induced micro-jets from thin liquid films. *Microfluid. Nanofluid.* **11**, 1–9 (2011)
18. M. Duocastella, J.M. Fernández-Pradas, J.L. Morenza, P. Serra, Droplet printing through bubble contact in the laser forward transfer of liquids. *Appl. Surf. Sci.* **257**, 2825–2829 (2011)